Steel and Composite Structures, *Vol. 33, No. 1* (*2019*) *111-122*
DOI: https://doi.org/10.12989/scs.2019.33.1.111

Post-fire test of precast steel reinforced concrete stub columns under eccentric compression

Yong Yang [1], Yicong Xue*[1,2], Yunlong Yu [1,3] and Zhichao Gong [1]

[1] *School of Civil Engineering, Xi'an University of Architecture and Technology, Shaanxi, China*
[2] *School of Natural and Built Environment, Queen's University Belfast, Northern Ireland, UK*
[3] *Key Lab of Structural Engineering and Earthquake Resistance, Shaanxi, China*

(*Received March 9, 2019, Revised July 11, 2019, Accepted September 27, 2019*)

Abstract. This paper presents an experimental work on the post-fire behavior of two kinds of innovative composite stub columns under eccentric compression. The partially precast steel reinforced concrete (PPSRC) column is composed of a precast outer-part cast using steel fiber reinforced reactive powder concrete (RPC) and a cast-in-place inner-part cast using conventional concrete. Based on the PPSRC column, the hollow precast steel reinforced concrete (HPSRC) column has a hollow column core. With the aim to investigate the post-fire performance of these composite columns, six stub column specimens, including three HPSRC stub columns and three PPSRC stub columns, were exposed to the ISO834 standard fire. Then, the cooling specimens and a control specimen unexposed to fire were eccentrically loaded to explore the residual capacity. The test parameters include the section shape, concrete strength of inner-part, eccentricity ratio and heating time. The test results indicated that the precast RPC shell could effectively confine the steel shape and longitudinal reinforcements after fire, and the PPSRC stub columns experienced lower core temperature in fire and exhibited higher post-fire residual strength as compared with the HPSRC stub columns due to the insulating effect of core concrete. The residual capacity increased with the increasing of inner concrete strength and with the decreasing of heating time and load eccentricity. Based on the test results, a FEA model was established to simulate the temperature field of test specimens, and the predicted results agreed well with the test results.

Keywords: precast steel reinforced concrete columns; reactive powder concrete; fire condition; post-fire residual capacity; eccentric compression

1. Introduction

Due to some favorable characteristics, including great stiffness, high bearing capacity and outstanding deformability, steel reinforced concrete (SRC) structures have been currently used in high-rise and large-span structures (Chu *et al.* 2018, Hajjar 2002). Nevertheless, the construction of traditional cast-in-place SRC structures involve the construction procedures both of reinforced concrete (RC) structures and steel structures, which is complex when SRC structures are applied in conventional multiple-story buildings. Meanwhile, precast concrete (PC) structures have been widely applied due to the high efficiency and controllable construction quality, which can be a solution to the problem of wasted resources for on-site construction (Kurama *et al.* 2018). In order to combine the advantages of PC structures and cast-in-place SRC structures, many researchers have proposed entirely precast SRC structures to facilitate the construction process of traditional SRC structures (Kim *et al.* 2013). In their structural system, entirely precast vertical members which are large in dimensions with heavy dead-weight are used, which will lead to an extra cost for employing special large vehicles and cranes in the process of transportation and installation. Furthermore, it might be difficult to ensure the structural integrity of beam-column joint area.

In order to solve the problems aforementioned, partially precast SRC members were proposed as an alternative method which can reduce the dead-weight of vertical precast SRC members, such as columns and shear walls. As shown in Fig. 1, the authors have proposed an innovative partially precast steel reinforced concrete (PPSRC) structure, in which structural components are composed of PPSRC columns, PPSRC beams, PPSRC joints and steel-concrete composite slabs. In the PPSRC frame system, beam members (PPSRC beam) can be fabricated by a precast high-strength U-shape shell and a cast-in-place beam core, and the mechanical behavior of PPSRC beams has been investigated by the authors (Yang *et al.* 2016). As for the vertical structural members, two kinds of innovative precast SRC columns, namely the hollow precast steel reinforced concrete (HPSRC) column and partially precast steel reinforced concrete (PPSRC) column, are introduced here. In the PPSRC column, the precast outer-part cast using steel fiber reinforced reactive powder concrete (RPC) can be prefabricated in workshop for better curing, and the cast-in-place column core can be cast together with the PPSRC beam core and slabs using conventional concrete on construction site to enhance the structural integrity and to

*Corresponding author,
Ph.D. Candidate, Research Associate,
E-mail: xjdxyc@foxmail.com

http://www.techno-press.org/?journal=scs&subpage=6
ISSN: 1229-9367 (Print), 1598-6233 (Online)

save the consumption of expensive RPC. In the HPSRC column, the core area is kept hollow to further reduce the column deadweight, meanwhile, the HPSRC column can be regarded as the formwork of inner-part of PPSRC column on site. Although the mechanical and seismic behavior of PPSRC and HPSRC columns has been conducted by the authors, the post-fire performance of these composite columns needs to be further explored (Yang *et al.* 2018).

Fire can be regarded as a significant hazard during the service period of building structures, and it is an essential requirement of any building design to maintain structural integrity during fire attack. In the past decades, many researchers have explored the fire and post-fire behavior of composite columns (Ye *et al.* 2019, Zhou and Han 2018, Chen *et al.* 2018, Tang 2017, 2018, Ukanwa *et al.* 2017, Won *et al.* 2016, Han *et al.* 2015, 2016, Leong *et al.* 2016, Espinos *et al.* 2014, Zaharia and Dubina 2014), nevertheless, most of the aforementioned researches concentrated on the fire performance of concrete filled steel tube (CFST) columns, in which steel reinforcements were exposed to the elevated temperature directly, and the fire performance of SRC columns has seldom been investigated. Han *et al.* (2015) explored the behavior of SRC columns after exposure to fire, and the test result indicated that the tested SRC columns behaved in a relatively ductile manner under fire. Nevertheless, in their study, the concrete types and strength grades along the cross section were uniform. Zhou and Han (2018) investigated the behavior of concrete-encased CFST columns under full-range fire including heating phase and cooling phase, but in their research, the inner tube was cast using high-strength concrete and the outer concrete was conventional normal-weight concrete, which is different from the proposed PPSRC and HPSRC columns in design philosophy. In the proposed columns, steel fiber reinforced reactive powder concrete is applied in the outer part to enhance the load-bearing capacity and durability, but reactive powder concrete may be more vulnerable to fire-induced spalling owing to the lowpermeability which may cause a rapid loss of concrete cover during the fire (Abdulraheem and Kadhum 2018). Meanwhile, the effects of cast-in-place conventional concrete of PPSRC columns and hollow core of HPSRC columns on the heat transfer should be further investigated.

Set against the aforementioned background, a series of tests were carried out on the representative specimens of building assemblies to investigate their behavior after exposure to the ISO834 standard fire. This paper presents the test results of three HPSRC stub columns and three PPSRC stub columns exposed to standard fires for different fire duration and then subjected to eccentric compression test after cooling. Compared with the PPSRC control stub column unexposed to fire, the effects of section shape, concrete strength of inner-part, eccentricity ratio and heating time on residual strength and deformability were critically investigated. On the basis of test results, corresponding finite element analysis (FEA) models of PPSRC columns and HPSRC columns were established to simulate the temperature distribution.

2. Experimental program

2.1 Specimen design

Three HPSRC stub columns and four PPSRC stub columns were designed and fabricated. All seven specimens had the same sectional dimensions except for the HPSRC specimens with a hollow core, and the key parameters were summarized in Table 1. Both the height and width of column cross section were 300 mm, and the entire column height was 1540 mm including a bottom steel plate with a thickness of 20 mm. The steel shape of all specimens was cruciform, which was welded by two HN175×90×5×8 steel of Q235 grade per the Chinese codes. For each part of the steel shape, the total height of steel flange and web were 90 mm and 175 mm, respectively, and the thickness of steel flange and web were 8 mm and 5 mm, respectively. For the steel reinforcements, all specimens were reinforced by 12 hot-rolled ribbed steel bars with a diameter of 20 mm of HRB400 grade per the Chinese codes. For the stirrups, all

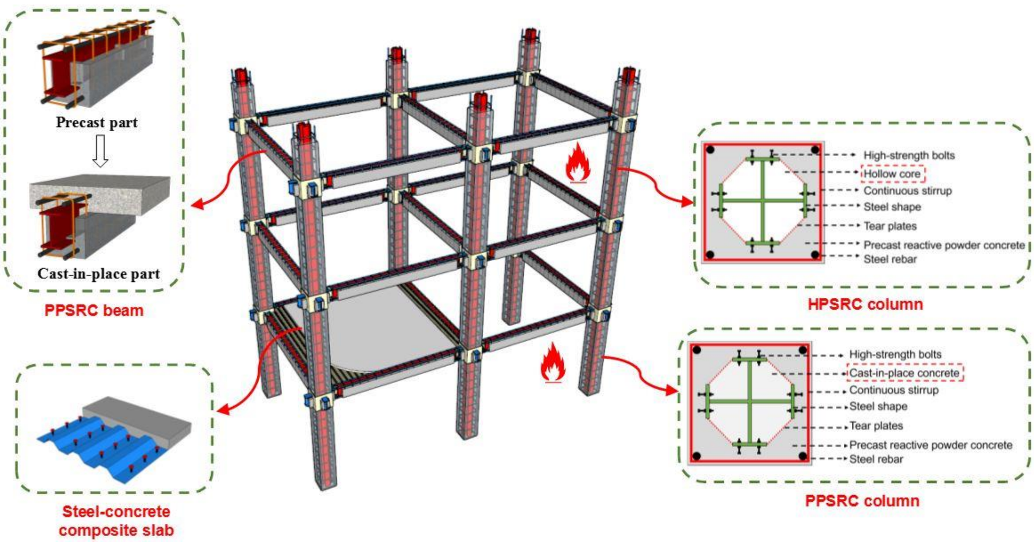

Fig. 1 General view of PPSRC structure

Table 1 Test matrix

Specimen ID	$b \times h$ /mm	Steel reinforcements			Concrete		e/h	t /min
		Steel shape (ρ_{ss})	Steel bar (ρ_{sl})	Stirrup (ρ_s)	$f_{c,\,out}$ /MPa	$f_{c,\,in}$ /MPa		
HPSRC-1	300×300	2 HN175×90×5×8 (4.94%)	4 20 (1.39%)	8@65 (1.14%)	96.8	-	0.2	120
HPSRC-2	300×300	2 HN175×90×5×8 (4.94%)	4 20 (1.39%)	8@65 (1.14%)	96.8	-	0.4	120
HPSRC-3	300×300	2 HN175×90×5×8 (4.94%)	4 20 (1.39%)	8@65 (1.14%)	96.8	-	0.6	120
PPSRC-1	300×300	2 HN175×90×5×8 (4.94%)	4 20 (1.39%)	8@65 (1.14%)	96.8	23.1	0.2	120
PPSRC-2	300×300	2 HN175×90×5×8 (4.94%)	4 20 (1.39%)	8@65 (1.14%)	96.8	23.1	0.2	150
PPSRC-3	300×300	2 HN175×90×5×8 (4.94%)	4 20 (1.39%)	8@65 (1.14%)	96.8	96.8	0.2	120
PPSRC-4	300×300	2 HN175×90×5×8 (4.94%)	4 20 (1.39%)	8@65 (1.14%)	96.8	23.1	0.2	0

*ρ_{ss} is steel shape ratio, ρ_{sl} is longitudinal reinforcement ratio, ρ_s is volumetric stirrup ratio, $f_{c,\,out}$ is compressive strength of outer-part concrete, $f_{c,\,in}$ is compressive strength of inner-part concrete, e/h is eccentricity ratio, t is time of fire exposure

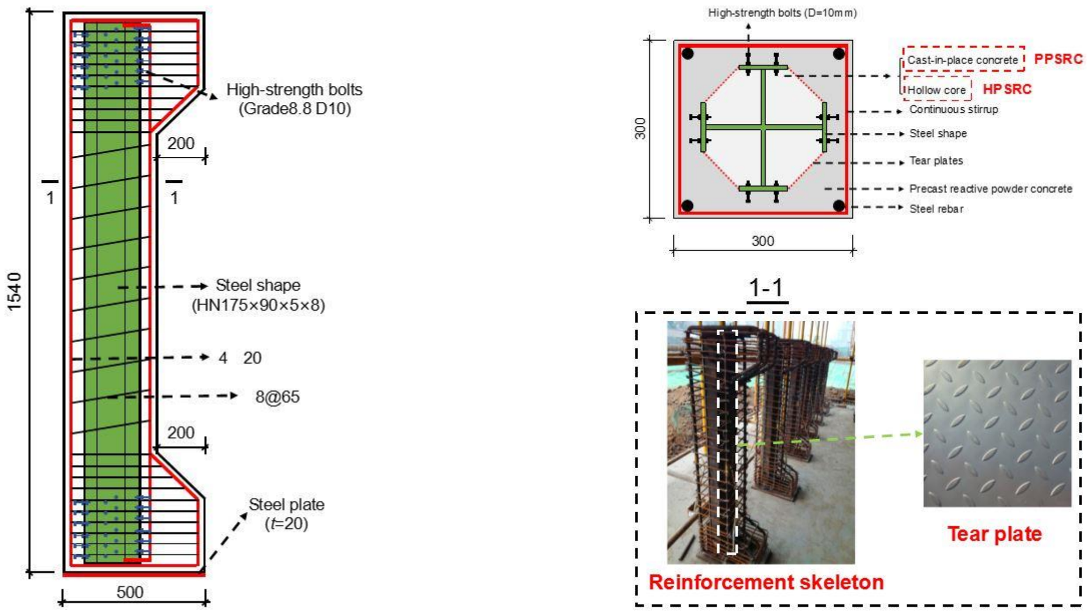

Fig. 2 Test specimens

specimens were confined by continuous rectangle stirrups with a diameter of 8 mm of HPB300 grade per the Chinese codes, and the spacing of adjacent stirrups was 65 mm. In order to avoid the local compressive failure, corbels were designed in the column top and bottom, and dense stirrups were arranged in the corbels. The design details can be found in Fig. 2.

In this research, all PPSRC specimens were fabricated by two steps, namely the precast step and cast-in-place step. In the precast step, the outer-part was prefabricated, which was composed of a cruciform steel shape, longitudinal steel bars, continuous rectangle stirrups and steel reinforced reactive powder concrete, and in this step, tear plates were assembled between the adjacent steel flanges by means of dot welding to be the inner formwork of RPC and to improve the bonding behavior. To further improve the bonding performance between the steel shape, inner concrete and outer concrete, some high-strength bolts were installed through the drilled holes on steel flanges. Because the bolt head was in the outer concrete and the bolt rear was in the inner concrete, the deformation of steel shape, inner concrete and outer concrete could be compatible. In the cast-in-place step, the concrete of column core was cast using conventional concrete to save the consumption of expensive RPC. The construction of HPSRC specimens only involve the first step aforementioned.

2.2 Material properties

The applied RPC was designed as C100 grade, indicating that the compressive strength was around 100 MPa, and the matrix compositions are displayed in Table 2. A 2% volume incorporation of steel fiber is used in RPC and the mechanical properties of applied steel fiber are shown in Table 3. The strength grades of inner conventional concrete were designed with three different levels, namely C30, C50 and C100, respectively. A number of RPC and concrete prisms with dimensions of 150 mm×150 mm×300 mm were prepared and tested in axial compression at the same time as the column tests. The measured average compressive strength of RPC coupons was 96.8 MPa, andthose of conventional concrete coupons were 24.3 MPa,

Table 2 Mix proportions of RPC

P.O. Cement	Mineral powder	Fly ash	Silica fume	River sand	Quartz sand	Super plasticizer	Steel fiber	W/B
1	0.1	0.2	0.15	0.8	0.5	0.003	0.2	0.22

*The ratio of steel fiber is volume ratio, and ratios of other components are weight ratios

Table 3 Material properties of steel fiber

Type	Length /mm	Diameter /mm	Tensile strength /MPa
Straight	13.0	0.2	2850

Table 4 Material properties of steel reinforcements

Reinforcements	Type	Grade	f_y /MPa	f_u /MPa
Transverse	8	HPB300	405.3	542.3
Longitudinal	20	HRB400	460.5	603.8
Steel shape	Web	Q235	275.4	396.8
	Flange		309.3	436.5

47.6 MPa and 96.8 MPa of C30, C50 and C100 grade, respectively. The mechanical properties of steel reinforcements were recorded in Table 4.

2.3 Test device and instrumentation

The tests were conducted in the *State Key Laboratory of Subtropical Building Sciencein South China University of Technology*, P.R. China. As shown in Fig. 3(a), the test system consisted of a gas furnace, which was used to heat the test specimens, a steel reaction frame and a hydraulic jack of 1800 kN in bearing capacity. The gas furnace is composed of an automatic fire control system and a heating chamber, of which the interior faces' area is 4000 mm×3000 mm and the height is 1500 mm. The temperature in the chamber was measured by eight thermocouples distributed uniformly in the furnace room. Because all specimens applied high-performance outer part and were medium-scale, the design axial capacities of test specimens were much greater than that of the loading apparatus. Therefore, the effect of axial load was ignored and all specimens were heated without axial compression.

The temperature inside the gas furnace was controlled by gas burners, and four K-type (nickel chromium-nickel silicon) thermocouples of 3 mm in diameter were mounted at the mid-height of specimens to monitor the temperature development at different locations. As shown in Fig. 4(a), thermocouples T1 and T2 were mounted in concrete, and thermocouples T3 and T4 were installed on the surface of steel shape. For HPSRC specimens, the thermocouple T3 was eliminated due to the hollow core.

All post-fire specimens were tested under eccentric compression with different load eccentricities. As shown in Fig. 3(b), the compressive load was applied by a compression machine with a maximum bearing capacity of 18000 kN. Before the specimens were loaded, knife edge plates were placed on the column top and bottom to provide the required end eccentricity. Five linear variable displacement transducers (LVDTs) were applied along the column height to measure the lateral deflections of test specimens. As illustrated in Fig. 4(b), five strain foils were mounted on the east surface of each specimen to monitor the strains of mid-height cross section.

2.4 Test procedure

As shown in Fig. 3(a), before heated, the corbels of columns were jacketed by fire-resistant coating and then wrapped by fire-resistant cotton to ensure the corbels arestrong enough in the post-fire eccentric loading,

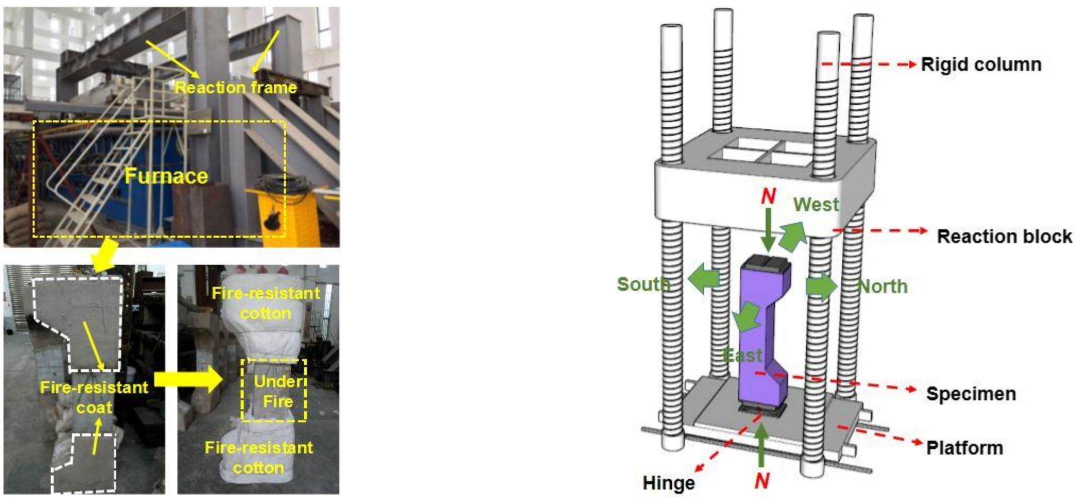

(a) Gas furnace (b) Static loading device

Fig. 3 Test devices

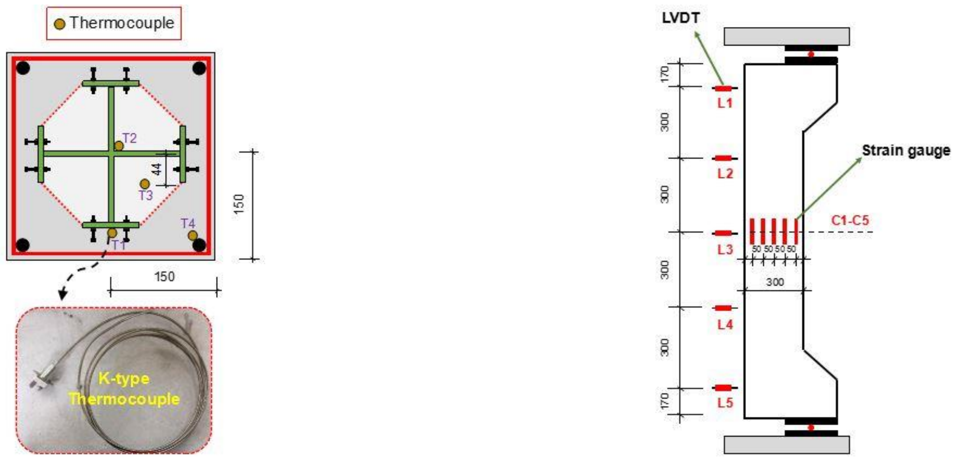

(a) Layout of thermocouples (b) Layout of LVDTs and strain foils

Fig. 4 Layout of gauges

indicating that only the mid-part of test columns was exposed to fire. During the heating process, the heating protocol was controlled by computer to ensure that the average temperature of the thermocouples in the gas furnace at different positions could agree with the ISO-834 standard temperature-time relationship. The elevated temperature lasted for 120 mins and 150 mins for different specimens. When the columns were heated to the target fire exposure time, the furnace chamber was opened 24 hours later. The columns were lifted out of the chamber and then cooled down gradually by the ambient air.

After cooled down, all specimens were eccentrically loaded to failure on a compression device, and the peak load for each column during the eccentric compression test stage was regarded as the post-fire residual capacity. The load was applied, using displacement control, at a loading rate of 0.005 mm per second before the specimens reached the corresponding peak loads and at a loading rate of 0.003 mm per second after the peak loads reached. Finally, the test terminated when the vertical load fell by more than 25% of the maximum experienced load or the lateral deflection was too large. The eccentric compression test of the control specimen PPSRC-4 followed the same test procedure.

3. Results and discussions of specimens after high temperatures

3.1 Test phenomenon and crack patterns

Because there was no high-temperature camera system in the gas furnace, the test observations and crack patterns of specimens subjected to fire condition were recorded when the specimens cooled down. As shown in Fig. 5, generally, all specimens kept intact without obvious deformation. In the most specimens, the color of column surfaces became greyish white after fire, and in few specimens, the surface color exhibited dark brown, indicating that these surfaces were near to the burner. Meanwhile, no explosive spalling was found in the precast RPC outer shell of all specimens due to the applied steel fibers, although decarbonization could be captured in some steel fibers near the column surface. Additionally, abundant temperature-induced cracks were observed on the column surface, and the width of some large cracks exceeded 1mm.

3.2 Temperature versus time relationships

The temperature variation in the internal cross section of test specimens was monitored by four thermocouples during the test process, and the results are plotted in Fig. 6. Thethermocouple T4, which located near the longitudinal

(a) HPSRC-1 (b) PPSRC-1 (c) PPSRC-2 (d) PPSRC-3

Fig. 5 Crack patterns after fire

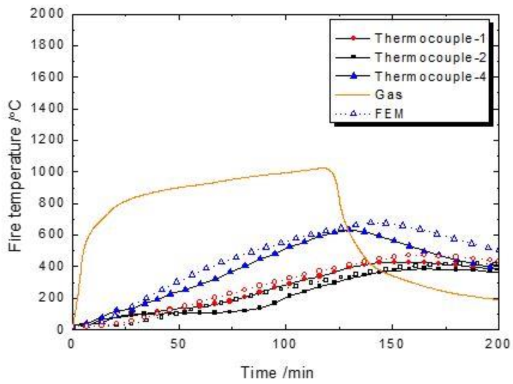

(a) HPSRC-1, HPSRC-2, HPSRC-3

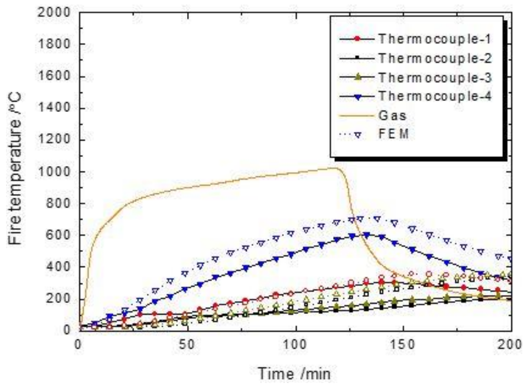

(b) PPSRC-1

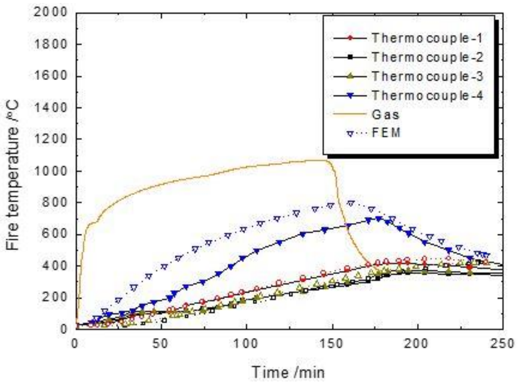

(c) PPSRC-2

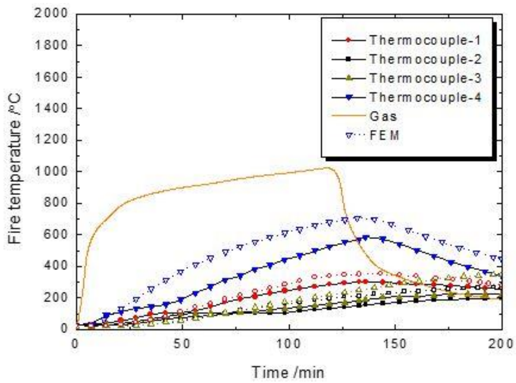

(d) PPSRC-3

Fig. 6 Measured and predicted temperatures with time

reinforcement, recorded the highest temperature in all thermocouples due to its 2-sides exposure to fire, and the thermocouple T2, which was installed at the center of cross section, recorded the lowest temperature due to the high thermal capacity and low thermal conductivity of concrete, which slowed down the heat penetration to the inner concrete layer. Meanwhile, the trends in Fig. 6 indicated that a temperature plateau could be observed at approximate 100°C, indicating the rise rate of temperature in the columns slowed down, which was more striking in the thermocouples located far away from the column surface. This temperature plateau could be primarily attributed to a large amount energy consumption through the water evaporation in concrete. In this research, the humidity of applied concrete was not measured and ignored in the above analysis. In future works, the effect of concrete humidity on the temperature distribution of these two composite columns will be explored.

As indicated in Fig. 6, when the heating process stopped, all measured temperatures did not descend immediately, and the time when the temperature fell occurred later in the inner column layer. A review of the measured temperatures showed that the entire cross section has not been completely cooled down at 60 mins after the heating process terminated. In this period, only the outer concrete was in the cooling phase, whereas the measured temperature by thermocouples T2 and T3 elevated at a low rate, and this phenomenon could be attributed to the insulation or thermal hysteresis effect of inner concrete.

Table 5 records the measured highest temperature which the specimens experienced. It can be seen from Table 5 that the temperature in the column core remained low throughout the fire duration due to the insulation effect of concrete, especially in PPSRC specimens. The measured temperatures by thermocouples T1 and T2 of PPSRC specimens and HPSRC specimens were similar at the early heating process, but HPSRC specimens suffered higher temperature at the points T1 and T2 than PPSRC specimens after heated for 60 mins owing to the heat convection and radiation in the hollow core. As shown in Table 5, by the comparison of specimens PPSRC-1 and PPSRC-2, it can be concluded that the measured temperature increased with the increasing of heating time, and by the comparison of specimens PPSRC-1 and PPSRC-3, it can be seen that the strength of inner concrete did not affect the temperature distribution and development obviously.

4. FE modelling of temperature field

The commercial FEA program ABAQUS software was applied here to establish the analytical model for temperature field prediction. Descriptions on the thermal properties for steel and concrete at high temperatures, element type, and other modelling techniques are introduced subsequently.

Thermal properties of steel reinforcements and inner concrete, including thermal conductivity, specific heat, and

Table 5 Test results

ID	t /min	Gauge	T_h /°C	T_{h-p} /°C	t_d /min	T_{d-p} /min	μ	N_r /kN
HPSRC-1	120	1	491.2	470.7	142	158	2.71	2378.8
		2	406.1	416.7	170	182		
		4	664.7	675.3	132	140		
HPSRC-2	120	1	498.1	470.7	142	158	3.60	1400.3
		2	410.6	416.7	165	182		
		4	645.9	675.3	134	140		
HPSRC-3	120	1	427.7	470.7	147	158	3.19	949.7
		2	387.9	416.7	168	182		
		4	632.1	675.3	133	140		
PPSRC-1	120	1	301.3	355.7	141	154	3.35	2873.0
		2	206.9	355.9	217	204		
		3	217.5	339.3	189	196		
		4	604.2	708.9	133	130		
PPSRC-2	150	1	416.3	444.9	189	218	3.32	2520.0
		2	356.1	422.9	248	240		
		3	375.2	420.8	214	242		
		4	700.9	800.6	164	161		
PPSRC-3	120	1	301.3	352.3	136	143	3.60	3060.3
		2	202.3	349.2	230	200		
		3	224.5	265.4	196	212		
		4	586.4	709.4	132	132		
PPSRC-4	0	-	-		-		3.63	4697.7

*t is time of fire exposure; T_h is measured highest temperature which specimen experienced; t_d is real time when measured temperature declined; T_{h-p} is predicted highest temperature which specimen experienced; t_{d-p} is predicted time when temperature declined; μ is ductility ratio, $\mu = \Delta_u / \Delta_y$, where parameters will be explained later in this paper; N_r is tested residual capacity

Table 6 Thermal properties of RPC

Thermal conductivity /(W/(m·°C))	Specificheat /(J/(kg·°C))	Thermalexpansion /(m/(m·°C))
$\lambda_c = 1.44 + 1.85\,exp(\frac{-T}{242.95})$	$c_c = \begin{cases} 950 & 20°C \leq T \leq 100°C \\ 950 + (T-100) & 100°C < T \leq 300°C \\ 1150 + \frac{(T-300)}{2} & 300°C < T \leq 600°C \\ 1300 & 600°C < T \leq 900°C \end{cases}$	$\Delta l / l = \begin{cases} 2.3 \times 10^{-11} T^3 + 9 \times 10^{-6} T - 1.8 \times 10^{-4} & 20℃ \leq T \leq 700℃ \\ 14 \times 10^{-3} & 700℃ < T \leq 1200℃ \end{cases}$

thermal expansion proposed by Eurocode 4 were adopted in this paper. For the thermal properties of reactive powder concrete, the thermal conductivity, specific heat, and thermal expansion proposed by Zheng *et al.* (2014) were applied here, as shown in Table 6.

The heat transfer 8-node brick element (DC3D8) was used for modelling concrete and steel shape, and the 2-node link element (DC1D2) was used for modelling steel reinforcements, including longitudinal rebar and stirrups. Because the corbels of specimens were coated by fire-resistant cotton, the corbels were not subjected to fire in the proposed FEA model, and the rest part was subjected to 4-sides fire. The thermal boundary conditions were defined according to the recommendations in Eurocode 4, as illustrated in Fig. 7(a). According to Eurocode 4, a constant convective heat transfer coefficient of 25 W/(m^2°C) was taken for the fire exposed edges and the corresponding thermal emissivity was taken as 0.7 for concrete surface. Tie constraint was adopted to simulate the interfaces between steel reinforcements, concrete and steel shape. According to some references, fibers can significantly enhance the spalling resistance of high performance concrete (Han *et al.* 2005). During the heating process, no obvious explosive spalling was captured in the precast RPC due to the application of steel fibers, therefore, the effect of explosive spalling was ignored in the proposed FEA model.

The above-described FEA model was validated by comparing the temperature variation with time predicted

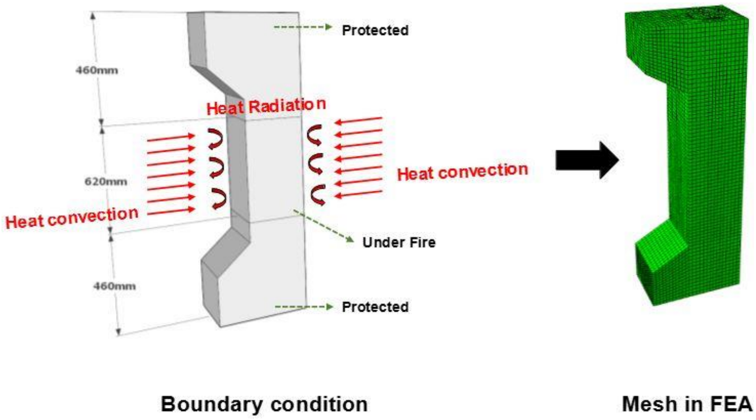

(a) Boundary condition

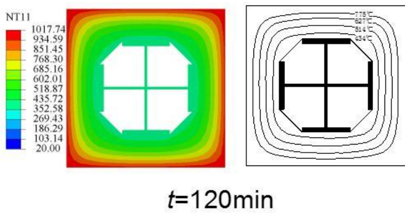

(b) Predicted temperature contour of HPSRC specimens

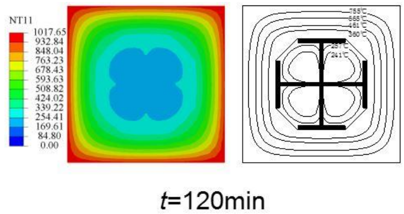

(c) Predicted temperature contour of PPSRC-1

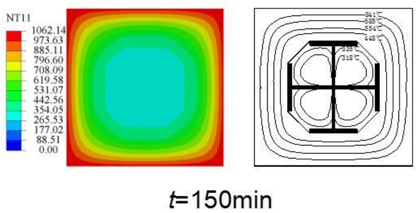

(d) Predicted temperature contour of PPSRC-2

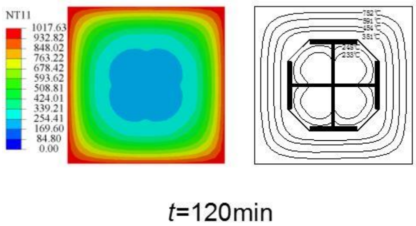

(e) Predicted temperature contour of PPSRC-3

Fig. 7 FEA modelling

from the developed model with the tested columns, as plotted in Fig. 6. Generally, the predicted temperature development agreed well with the measured results, but some difference could be found in the figure due to the water evaporation and thermal resistance between the steel shape and concrete, which did not be considered in the model for simplification. In the future, these details will be considered in the refined FEA model and a sensitivity study will be conducted to verify the simplification. Meanwhile, the highest temperature which specimens experienced occurred after the heating process stopped both in predicted and measured results, especially in the inner concrete layer, indicating that the column core was still heated even the temperature of environment began to descend, which might lead to inner damage.

The predicted temperature contours of test specimens were shown in Figs.7(b)-(e), in which the temperature contour of the specimen PPSRC-2 was drew at 150 mins from heating and the other contours were drew at 120 mins from heating. As shown in Fig. 7, it can be concluded that all the contours were rounded rectangles and close to circles near the column core. Meanwhile, the temperature at column corner was higher than that at column center at the same section height,indicating that the column corner might be more vulnerable in post-fire behavior.

5. Results and discussions of the eccentric loading test

5.1 Failure modes

The crack patterns and failure modes of post-fire tests were illustrated in Fig. 8, in which all photos were taken from the east side of test specimens, and the directions of surfaces were illustrated in Fig. 3(b). There were two typical types of failure modes occurred in PPSRC and HPSRC columns according to different eccentricity ratios, which were tension-controlled failure and compression-controlled failure.

Specimens HPSRC-1, HPSRC-2, PPSRC-1, PPSRC-2, PPSRC-3 and PPSRC-4 with low and medium eccentricity ratios suffered the compression-controlled failure. The failure process of these specimens could be divided into three stages. In the first stage, cracks in both compression and tension sides occurred, and these cracks continued to emerge and developed as the load increasing. The second stage began with the propagating and widening of these existing cracks, and many wide cracks formed in the compression area. In the final stage, the RPC shell in the compression side reached the corresponding ultimate compressive strain and began to crush and the load dropped

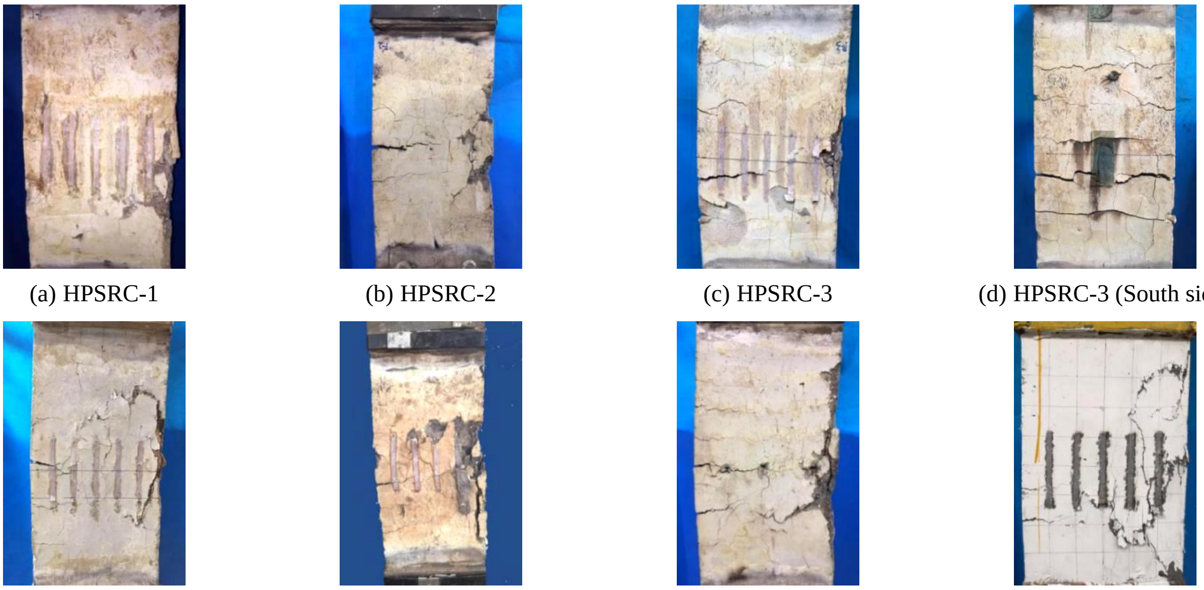

(a) HPSRC-1 (b) HPSRC-2 (c) HPSRC-3 (d) HPSRC-3 (South side)

(e) PPSRC-1 (f) PPSRC-2 (g) PPSRC-3 (h) PPSRC-4

Fig. 8 Failure modes and crack patterns

rapidly.

The specimen HPSRC-3 with the highest eccentricity ratio suffered the tension-controlled failure. During the test process, compared with other specimens, more severer cracks could be captured in the tension area. As the load increased, these cracks began to converge and then developed as main cracks, and numerous steel fibers were observed to be pulled out from the RPC matrix, while few visible cracks were observed in the compression area. Finally, as shown in Fig. 8(d), a major tensile crack suddenly formed and then the RPC in compression area began to split and the load dropped rapidly.

Generally, the larger crushing area and severer tensile cracks could be found in the specimens with longer heating process due to the severer inner damage. Some specimens were broken after test, and slight buckling of longitudinal reinforcements was found but the steel flanges still could be effectively confined without buckling.

5.2 Load-deflection curves

The load-lateral deflection curves of all specimens are plotted in Fig. 9. It can be concluded from Fig. 9 that all specimens were in elastic stage before loaded to $0.5N_r$, where N_r is the maximum residual capacity, and then the curves deviated from linear stage due to inner damage. When the specimens reached the corresponding maximum residual capacities, the curves suffered sudden drops due to the crushing of fire-damaged RPC shell. Nevertheless, the steel shape and inner confined concrete could effectively enhance the deformability and bear the post-peak load, all fire-damaged specimens behaved in a ductile manner after the peak loads reached.

By the comparison between the residual capacities of specimens HPSRC-1, HPSRC-2 and HPSRC-3, it can be concluded that the residual capacity increased with the decreasing of load eccentricity, and it is reasonable because the higher load eccentricity could lead to the higher additional bending moment. It can be also concluded that the failure mode changed from tension-controlled failure to compression-controlled failure with the decreasing of eccentricity ratio. By the comparison between the residual capacities of specimens PPSRC-1, PPSRC-2 and PPSRC-4, it can be concluded that the residual capacity increased with the decreasing of heating time. It is reasonable since the longer heating time induced more severe damage in test specimens. Meanwhile, by the comparison between the residual capacities of specimens HPSRC-1, PPSRC-1 and PPSRC-3, it can be found that the residual capacity increased with the increasing of inner concrete strength.

5.3 Ductility

Ductility is a basic index used to evaluate the deformability of structural members. Based on the load-lateral deflection curves shown in Fig. 9, the ductility ratio could be determined as the result of the deflection of ultimate point Δ_u divided by the deflection of yielding point Δ_y. Δ_u was defined as the lateral deflection of column when the load descended to 75% of the experienced maximum load in failure stage or the lateral deflection was too large. Δ_y was determined from the load-lateral deflection curves and based on an equal energy method. As illustrated in Fig. 10, a secant was made to intersect the load-lateral deflection curve at point A to ensure the shadow area A1 equals to the shadow area A2, and the projection of point B onto the curve was regarded as the yield point (Park 1988). The calculated ductility ratios of test specimens are recorded in Table 5. It can be seen from Table 5 that the ductility ratio increased with the decreasing of heating time and with the increasing of inner concrete strength and eccentricity ratio, except for the specimen HPSRC-3 with a high eccentricity ratio. The reason is that the test process of HPSRC-3 ended due to the visible severe damage and large deflection rather

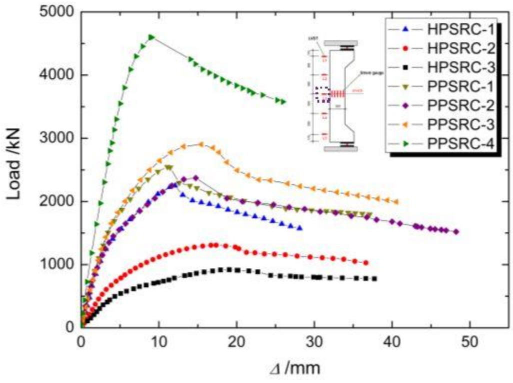

Fig. 9 Load-deflection curves

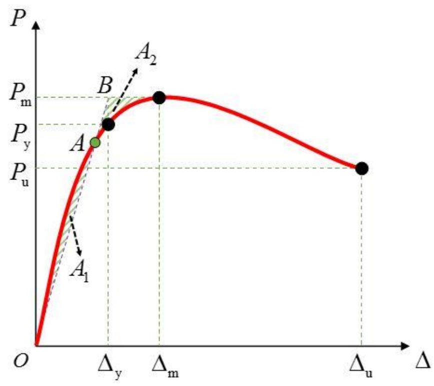

Fig. 10 Definition of ductility ratio

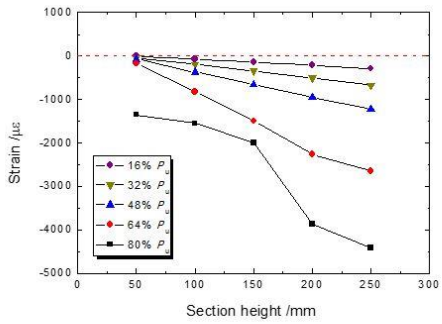

(a) HPSRC-1

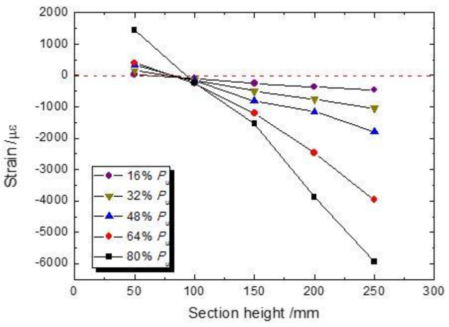

(b) HPSRC-2

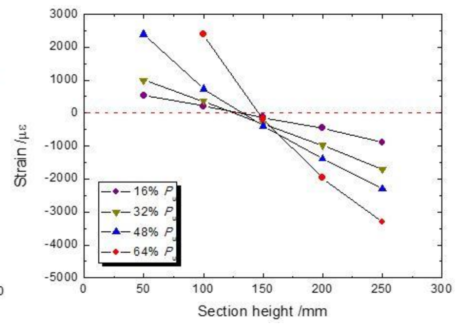

(c) HPSRC-3

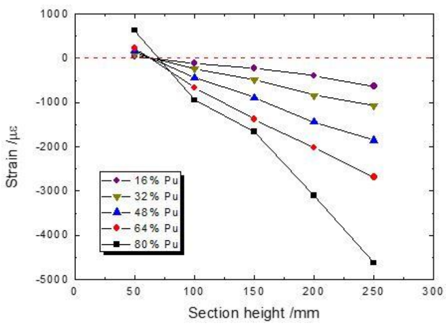

(d) PPSRC-1

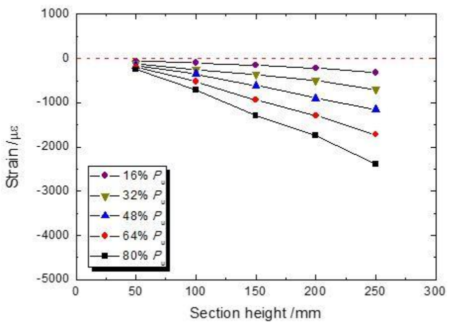

(e) PPSRC-3

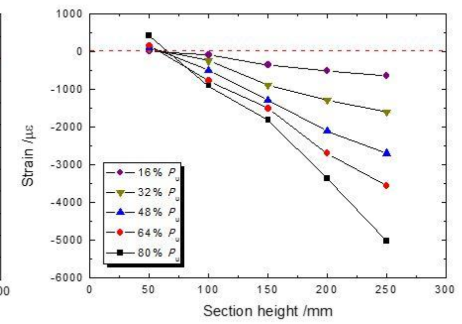

(f) PPSRC-4

Fig. 11 Strains along the column height

than the sudden load drop, indicating that the ductility ratio of HPSRC-3 could be higher than that of HPSRC-2 with a medium eccentricity ratio if it could be loaded further. Generally, all specimens exhibited satisfactory deformability even being fire-damaged.

5.4 Strain analysis

With the aim to verify the plane section assumption, a set of strain gauges were installed along the height of column cross section, and the arrangements of strain gauges were illustrated in Fig. 4(b). Fig. 11 shows the strain distribution curves of test specimens, and the result agreed well with the assumption, in which strain was distributed linearly along the column height during the test process. It also can be concluded from Fig. 11 that the tensile strains of specimens HPSRC-1, HPSRC-2, PPSRC-1, PPSRC-3 and PPSRC-4 did not exceed the tensile yield strain of longitudinal steel reinforcements, indicating that these specimens suffered compression-controlled failures.

6. Conclusions

This paper presents an experimental research on two innovative composite columns, namely the hollow precast steel reinforced concrete (HPSRC) column and partially precast steel reinforced concrete (PPSRC) column. A total of six stub column specimens were exposed to the ISO834 standard fire and then were eccentrically loaded with another control specimen without exposure to fire, focusing on the influence of test parameters of section shape, concrete strength of inner-part, eccentricity ratio and heating time. Based on the test results, FEA models were established through ABAQUS to explore the temperature distribution. Within the limitations of this paper, the following conclusions can be drawn:

- After fire, all specimens kept intact without obvious deformation. No explosive spalling was found in the precast RPC outer shell of all specimens due to the applied steel fibers, although decarbonization could be captured in some steel fibers near the column surface. Meanwhile, abundant temperature-induced cracks were observed on the concrete surface without spallation. The PPSRC columns experienced lower core temperature in fire as compared with the HPSRC columns due to the insulating effect of core concrete.
- Heat transfer analysis was carried out by the FEA model in ABAQUS to predict the temperature distribution of cross-section, and this model was validated through the measured temperature obtained from the tests. It can be concluded that all temperature contours were rounded rectangles and close to circles near the column core. Meanwhile, the temperature at column corner was higher than that at column center at the same section height, indicating that the column corner might be more vulnerable in post-fire behavior. In the current FEA model, the water evaporation and thermal resistance between the steel shape and concrete did not be considered for simplification. In the future, these details will be considered in the refined FEA model and a sensitivity study will be conducted to verify the simplification.
- There were two types of failure modes occurred in PPSRC and HPSRC specimens according to different eccentricity ratios, which were tension-controlled failure and compression-controlled failure. The specimens with low and medium eccentricity ratios suffered the compression-controlled failure, and the specimen with the highest eccentricity ratio suffered the tension-controlled failure, which could be verified by sectional strain analysis. Some specimens were broken after test, and slight buckling of the longitudinal reinforcements was found but the steel flanges still could be effectively confined without buckling.
- The residual capacity of PPSRC and HPSRC specimens increased with the decreasing of heating time and eccentricity ratio, and with the increasing of inner concrete strength. The ductility of test specimens follow the similar trends, except for the eccentricity ratio. The ductility and deformability enhanced with the increasing of eccentricity ratio.

Acknowledgments

The experiments are sponsored by the National Key Research and Development Program of China (Grant No. 2017YFC0703404), the National Natural Science Foundation of China (Grant No. 51578443 and No. 51778525), Potential Excellent PhD Dissertation Foundation of Xi'an University of Architecture and Technology (Grant No. 1601110035). The supports are greatly appreciated. Additionally, financial support from the China Scholarship Council (CSC) for Yicong Xue's research at QUB, as a visiting researcher, is highly appreciated.

References

ABAQUS (2016), ABAQUS 2016 Documentation, Dassault Systèmes, Providence, RI, USA.

Abdulraheem, M.S. and Kadhum, M.M. (2018), "Experimental and numerical study on post-fire behaviour of concentrically loaded reinforced reactive powder concrete columns", *Constr. Build. Mater.*, **168**, 877-892. https://doi.org/10.1016/j.conbuildmat.2018.02.123

BS EN 1994-1-2 (2005), Eurocode 4 - Design of composite steel and concrete structures - Part 1-2: General rules - Structural fire design, Brussels, Belgium.

Chen, Z., Liu, X. and Zhou, W. (2018), "Residual bond behavior of high strength concrete-filled square steel tube after elevated temperatures", *Steel Compos. Struct., Int. J.*, **27**(4), 509-523. http://dx.doi.org/10.12989/scs.2018.27.4.509

Chu, L., Li, D., Ma, X. and Zhao, J. (2018), "Cyclic behaviour of concrete encased steel (CES) column-steel beam joints with concrete slabs", *Steel Compos. Struct., Int. J.*, **29**(6), 735-748. http://dx.doi.org/10.12989/scs.2018.29.6.735

Espinos, A., Romero, M.L., Portolés, J.M. and Hospitaler, A. (2014), "Ambient and fire behavior of eccentrically loaded elliptical slender concrete-filled tubular columns", *J. Constr. SteelRes.*, **100**, 97-107. https://doi.org/10.1016/j.jcsr.2014.04.025

Hajjar, J.F. (2002), "Composite steel and concrete structural systems for seismic engineering", *J. Constr. Steel Res.*, **58**(5), 703-723. https://doi.org/10.1016/S0143-974X(01)00093-1

Han, C.G., Hwang, Y.S., Yang, S.H. and Gowripalan, N. (2005), "Performance of spalling resistance of high performance concrete with polypropylene fiber contents and lateral confinement", *Cement Concrete Res.*, **35**(9), 1747-1753. https://doi.org/10.1016/j.cemconres.2004.11.013

Han, L.H., Tan, Q.H. and Song, T.Y. (2015), "Fire performance of steel reinforced concrete columns", *J. Struct. Eng.*, **141**(4), 04014128. https://doi.org/10.1061/(ASCE)ST.1943-541X.0001081

Han, L.H., Zhou, K., Tan, Q.H. and Song, T.Y. (2016), "Performance of steel-reinforced concrete column after exposure to fire: FEA model and experiments", *J. Struct. Eng.*, **142**(9), 04016055. https://doi.org/10.1061/(ASCE)ST.1943-541X.0001511

ISO-834 (1975), Fire-resistance tests-Elements of building construction, Geneva, Switzerland.

Kim, S., Hong, W.K., Kim, J.H. and Kim, J.T. (2013), "The development of modularized construction of enhanced precast composite structural systems (Smart Green frame) and its embedded energy efficiency", *Energy Build.*, **66**(5), 16-21. https://doi.org/10.1016/j.enbuild.2013.07.023

Kurama, Y.C., Sritharan, S., Fleischman, R.B., Restrepo, J.I., Henry, R.S., Cleland, N.M., Ghosh, S.K. and Bonelli, P. (2018), "Seismic-Resistant Precast Concrete Structures: State of the Art", *J. Struct. Eng.*, **144**(4), 03118001. https://doi.org/10.1061/(ASCE)ST.1943-541X.0001972

Leong, S.H., Sulong, N.H.R. and Jameel, M. (2016), "Bolted connections to tubular columns at ambient and elevated temperatures - a review", *Steel Compos. Struct., Int. J.*, **21**(2), 303-321. http://dx.doi.org/10.12989/scs.2016.21.2.303

Park, R. (1988), "State of the art report ductility evaluation from laboratory and analytical testing", *Proceedings of 9th World*

Conference on Earthquake Engineering, Tokyo, Japan, August.
Tang, C.W. (2017), “Fire resistance of high strength fiber reinforced concrete filled box columns”, *Steel Compos. Struct., Int. J.*, **23**(5), 611-621. http://dx.doi.org/10.12989/scs.2017.23.5.611
Tang, C.W. (2018), “Fire resistance of high strength concrete filled steel tubular columns under combined temperature and loading”, *Steel Compos. Struct., Int. J.*, **27**(2), 243-253. http://dx.doi.org/10.12989/scs.2018.27.2.243
Ukanwa, K.U., Sharma, U., Hicks, S.J., Abu, A., Lim, J.B.P. and Clifton, C.G. (2017), “Behaviour of continuous concrete filled steel tubular columns loaded concentrically in fire”, *J. Constr. Steel Res.*, **136**, 101-109. https://doi.org/10.1016/j.jcsr.2017.05.011
Won, D.H., Han, T.H., Kim, S. and Kang, Y.J. (2016), “Fire resistance of double-skinned composite tubular columns including concrete confinement”, *Mater. Struct.*, **49**(4), 1269-1284. https://doi.org/10.1617/s11527-015-0575-9
Yang, Y., Yu, Y., Guo, Y., Roeder, C.W., Xue, Y. and Shao, Y. (2016), “Experimental study on shear performance of partially precast Castellated Steel Reinforced Concrete (CPSRC) beams”, *Steel Compos. Struct., Int. J.*, **21**(2), 289-302. http://dx.doi.org/10.12989/scs.2016.21.2.289
Yang, Y., Xue, Y., Yu, Y. and Gao, F. (2018), “Experimental study on seismic performance of partially precast steel reinforced concrete columns”, *Eng. Struct.*, **175**, 63-75. https://doi.org/10.1016/j.engstruct.2018.08.027
Ye, Z., Jiang, S., Heidarpour, A., Li, Y. and Li, G. (2019), “Experimental study on cyclically-damaged steel-concrete composite joints subjected to fire”, *Steel Compos. Struct., Int. J.*, **30**(4), 351-364. http://dx.doi.org/10.12989/scs.2019.30.4.351
Zaharia, R. and Dubina, D. (2014), “Fire design of concrete encased columns: validation of an advanced calculation model”, *Steel Compos. Struct., Int. J.*, **17**(6), 835-850. http://dx.doi.org/10.12989/scs.2014.17.6.835
Zheng, W., Wang, R. and Wang, Y. (2014), “Experimental study on thermal parameter of reactive powder concrete”, *J. Build. Struct.*, **35**(9), 107-114. [In Chinese] http://dx.doi.org/10.14006/j.jzjgxb.2014.09.014
Zhou, K. and Han, L.H. (2018), “Experimental performance of concrete-encased CFST columns subjected to full-range fire including heating and cooling”, *Eng. Struct.*, **165**, 331-348. https://doi.org/10.1016/j.engstruct.2018.03.042

CC